ARTICLE

Order–disorder transition in a two-dimensional boron–carbon–nitride alloy

Jiong Lu[1,2,*], Kai Zhang[1,2,*], Xin Feng Liu[4], Han Zhang[1,2], Tze Chien Sum[4], Antonio H. Castro Neto[2,3] & Kian Ping Loh[1,2]

Two-dimensional boron–carbon–nitride materials exhibit a spectrum of electronic properties ranging from insulating to semimetallic, depending on their composition and geometry. Detailed experimental insights into the phase separation and ordering in such alloy are currently lacking. Here we report the mixing and demixing of boron–nitrogen and carbon phases on ruthenium (0001) and found that energetics for such processes are modified by the metal substrate. The brick-and-mortar patchwork observed of stoichiometrically percolated hexagonal boron–carbon–nitride domains surrounded by a network of segregated graphene nanoribbons can be described within the Blume–Emery–Griffiths model applied to a honeycomb lattice. The isostructural boron nitride and graphene assumes remarkable fluidity and can be exchanged entirely into one another by a catalytically assistant substitution. Visualizing the dynamics of phase separation at the atomic level provides the premise for enabling structural control in a two-dimensional network for broad nanotechnology applications.

[1] Department of Chemistry, National University of Singapore, 3 Science Drive 3, Singapore 117543, Singapore. [2] Graphene Research Centre, National University of Singapore, 6 Science Drive 2, Singapore 117546, Singapore. [3] Department of Physics, National University of Singapore, 2 Science Drive 3, Singapore 117542, Singapore. [4] Division of Physics and Applied Physics, School of Physical and Mathematical Sciences, Nanyang Technological University, 21 Nanyang Link, Singapore 637371, Singapore. * These authors contributed equally to this work. Correspondence and requests for materials should be addressed to K.P.L. (email: chmlohkp@nus.edu.sg).

A common strategy for tuning the electronic properties of a solid state material is the incorporation of hetero-atoms in the bulk lattice[1–4]. The structural similarity between graphene (G) and h-BN motivates the alloying of the two to achieve ternary hexagonal boron–carbon–nitride (h-BC$_x$N) composite with tunable electronic properties[5–11]. However, the ability to undergo homophilic (C–C) as well as heterophilic (C–B, C–N and BN) in h-BC$_x$N generates a rich variety of polymorphic structures, making the precise control of their chemical stoichiometry and geometry formidable. Recently, patterned regrowth[12,13] has been attempted for the spatially controlled synthesis of lateral junctions between electrically conductive graphene and insulating h-BN to make integrated circuitry[12]. The successful interfacing of these two isoelectronic materials to form hybrid monolayer film on Ru was also demonstrated by Sutter et al. It is reported that the elimination of residual carbon adatoms is crucial to prevent unintentional intermixing of the G–BN interfaces[11]. In contrast to spatially segregated G–BN composite, intermixing of B, C and N atoms under thermodynamic non-equilibrium conditions may lead to semiconducting h-BC$_x$N alloys[9,14,15]. However, the precise conditions needed to control the stoichiometries of well-mixed h-BC$_x$N phases and the relation between crystallization and the ordering in such ternary two-dimensional (2D) alloy are far from understood.

Here, we carry out a systematic scanning tunneling microscopy (STM) study to understand the dynamics of mixing and order–disorder transition in the ternary h-BC$_x$N system with a view towards understanding their atomic and electronic structures. We demonstrate the conditions under which different polymorphic structures can be obtained, including phase-modulated mosaic-like film and stoichiometrically percolated h-BC$_2$N alloy. The complex pattern observed in 2D h-BC$_x$N system can be well-described using Blume–Emery–Griffiths (BEG) model[16] with the introduction of at least two order parameters (density and sublattice ordering). The insights into the phase separations and order–disorder transition described here are generic for the growth of a large class of 2D alloys.

Results

Mixing and demixing of BN and C phases on Ru(0001). The energetics of surface mixing and segregation in 2D monolayers are mediated heavily by the metallic substrate[17–19], the latter can have the role of a catalyst as well as a solvent at high temperature. Through grain boundaries and exposed edges, gaseous species can intercalate between the 2D films and the metal substrate and be catalytically decomposed at elevated temperatures to form active elemental dopants. The lower energy barrier of surface diffusion on metal relative to bulk diffusion in the host lattice, and surface-catalysed displacement of atoms from its host lattice enhance intermixing relative to thicker films. In the case of graphene on Ru(0001) (G-Ru), the substitution of heteroatoms into the graphene matrix could be modulated spatially by the moiré superstructure, which influences the anisotropic phase segregation in periodic segregation sites. Owing to the buckling instability of graphene on Ru, some carbon atoms are displaced vertically from the substrate, while others remain attached, forming a graphene landscape of humps and valleys (Fig. 1a). Strong chemical hybridization between the Ru substrate and the carbon atoms attached to it results in a significant electron enrichment, potentially increasing the reactivity towards heteroatomic exchange.

To create the conditions for the substitution of N and B atoms into the G-Ru, a sub-monolayer (∼0.8 l) graphene was first grown on Ru(0001). This was used subsequently as the reaction template for reacting with vaporized borazine at 900 K. We found that below 850 K, there is insufficient thermal energy to overcome

the energy barrier of atomic exchange. Aided by Ru-catalysed processes, interpenetrated h-BC$_x$N phases can be grown at temperature above 850 K. In the initial stage, the substitution and etching of graphene proceeds at the grain boundaries and edges (Fig. 1a,b and Supplementary Fig. S1), where borazine molecules are catalytically decomposed by Ru to release highly reactive N, B and H species. Atomic H generated from the catalytic decomposition participated in the etching of carbon atoms. This process can be described using the reaction equation as shown below:

$$G + B_3N_3H_3 \overset{Ru}{\Rightarrow} BC_xN + CH_x \uparrow \qquad (1)$$
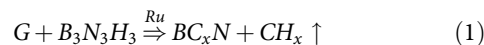
at a low dose of borazine 5 Langmuir (L), a mosaic-like patchwork consisting of interconnected mortar threads running in a zigzag conformation appears on the surface (Fig. 1c–f and Supplementary Fig. S2). In the work reported by Sutter et al.[11], shallow lines were imaged in the mixed BCN (boron–carbon–nitride) regions. These lines appeared to be relatively disordered and their atomic structures and chemical composition were unknown. In contrast, the thread observed here aligns with the $<11\bar{2}0>$ orientations of graphene and zigzags at 120° with a periodicity of ∼6 nm, which is approximately twice of the lattice constant of the graphene moiré pattern a ($a = 2.97$ nm). Atomic-resolved imaging and growth studies under C-rich or BN-rich conditions allow us to deduce the threads to be made of phase-segregated graphene and the encircled dark regions to be mixed h-BC$_x$N phases. The threads have widths of 0.49 nm and an atomic lattice constant of 0.247 nm, which is close to that of graphene. In the penetration of B/N into the graphene lattice to form the BC$_x$N phase, some carbon atoms are preferentially phase-segregated into the periphery of the domains, where it forms the interconnected mortar thread network (graphene nanoribbons: GNRs) encircling individual h-BC$_x$N bricks. The relatively flat region in Fig. 2e ranging from −0.1 to 0.5 eV in the scanning tunneling spectroscopy (STS) spectra recorded on GNRs suggests the occurrence of energy gaps of ∼0.6 eV, which might be due to the quantum confinement or the breakage of lattice symmetry induced by strong interactions with Ru substrate (see Supplementary Figs S3 and S4 and Supplementary Note 1 for details). Interestingly, we observe a dynamic unstitching of the GNRs as the inner BCN domain grows: the length of the bright triangles expands by multiples of a even as their overall density decreases. The spatial topology of the mortar threads follows the symmetry of graphene moiré pattern, thus yielding a triangular motif (Fig. 1c–f). The fact that these mortar threads are composed of carbon can be judged from its decreased coverage on the surface upon B/N enrichment, and increased coverage after carbon enrichment at 900 K. The occurrence of the brick-and-mortar structure observed here describes the classic segregation of solute at sinks such as grain boundary, dislocation and free surface, which is analogous to the so-called Cottrell atmospheres created by clouds of impurity atoms near dislocations in crystals[20]. The segregation sites aligning with the centre of moiré humps are the most accessible and energetically favourable sink for carbon segregants. The interfacial strain induced by lattice mismatch between graphene and h-BC$_x$N drives the rippling of GNRs with an average apparent height of 0.5 Å to relax the internal stress.

The mosaic patchwork formed by GNRs and h-BC$_x$N domains are structurally fluid and the substitution of graphene by BN (Fig. 1), or vice versa, are reversible (Fig. 2), depending on the excess of chemical potentials in the growth conditions. The GNRs increase in density at increasingly C-rich conditions (Fig. 2f–h) attained by dosing hydrocarbon. If the density of the carbon phase exceed a certain threshold, for example, 60 at%,
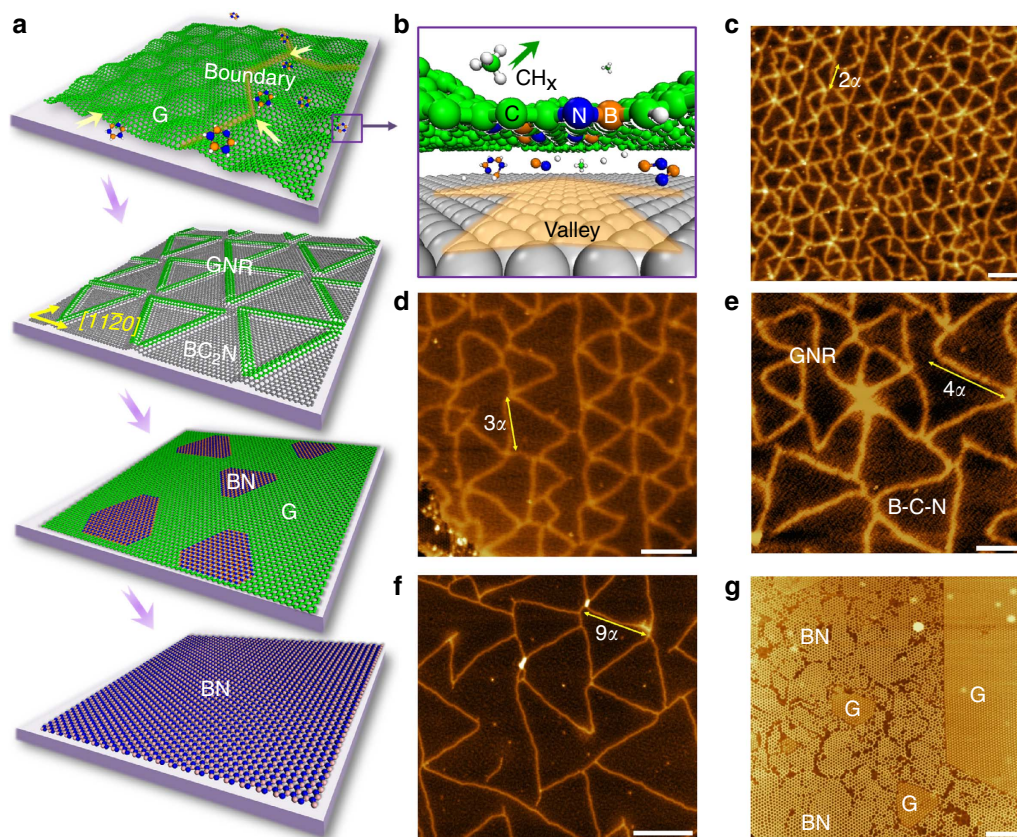
Figure 1 | Formation of mixed BCN domains enclosed by GNRs. (a) Illustration of the substitutional doping of G/Ru(0001) by borazine leading to the formation of brick-and-mortar pattern, domain-wise G-BN mosaic film and a complete replacement of G into BN. **(b)** Schematic shows the subsurface diffusion and catalytic decomposition of borazine to generate active B and N species which replace lattice carbon in graphene; **(c)** Phase-segregated GNRs modulated by the moiré superlattice, encircling the mixed h-BC$_x$N domains to form brick-and-mortar pattern. The generation of a triangular GNR superstructure with a lattice constant of 6 nm $\approx 2a$ (a: lattice constant of graphene moiré superstructure on Ru(0001)) with the borazine dosage of 5 Langmuir (L). **(d–f)** STM images show the evolution of mixed BCN domains (dotted dark regions) and demixed GNR phases (bright lines) upon the stepwise dosing of borazine at 900 K. The average side lengths of GNR triangles are increased from $3a$ to $4a$ and $9a$ with the increase of the dosage of borazine from 10 to 20 l. **(g)** The formation of domain-wise G-BN composite by a complete phase segregation in BC$_x$N at 900 K (borazine: 100 l). Scale bars in **(c–g)** are 6, 10, 6, 25 and 40 nm, respectively.

(Supplementary Fig. S5) besides a dense triangular network of GNR arrays (Fig. 2g), the appearance of moiré humps due to a complete replacement of the BN phase by graphene phase occurs. The brick-and-mortar film can be repaired to form a highly ordered graphene moiré pattern after additional C$_2$H$_4$ dosage and prolonged annealing to reach a complete equilibrium (Fig. 2j).

Structural characterization. Within the brick-and-mortar structure, high-resolution imaging of the enclosed h-BC$_x$N phase reveals a quasi-random distribution of bright spots embedded in a dark triangular lattice with a lattice constant of ~ 2.5 Å (Fig. 3). These bright spots have the same STM contrast as that of carbon atoms imaged in GNRs (Fig. 2a–d), although the triangular lattice hosting the bright spots has nearly the same lattice constant and image contrast as that of valley regions of BN nanomesh grown on Ru(0001)[21]. Therefore, the bright dot is attributed to a local enhancement of density of states presumably due to carbon doping, which is evidenced by the appearance of a mid-gap state close to Fermi level in the STS spectrum (Fig. 3e). The intensity of this peak at ~ -0.1 eV is greatly enhanced when STS is conducted at a cluster of bright spots (Fig. 3e), which may be due to the overlapping of states from carbon dopants (see Supplementary Figs S5 and S6 for details). This assignment also rationalizes the observation of a bias-dependent tunnelling image

contrast in the h-BC$_x$N lattice (Supplementary Fig. S7). Close examination reveals that the carbon atoms (bright spots) have a tendency to align in three equivalent crystallographic directions with a lattice spacing of 2.5 Å, as observed in FFT (Fast Fourier Transform) of the large-scale STM image (Fig. 3b). Hence, alloyed h-BC$_x$N displays a paracrystalline phase with short-range order. The tendency for ordering is known to be particularly low in hexagonally packed surface alloys because of the relatively high degeneracy of different states with similar composition. The integrated area of bright spots (carbon atoms) is nearly equal to that of dark region (BN) (49.5%:50.5%), which indicates that a stoichiometrically percolated h-BC$_2$N alloy is obtained upon substitutional doping (Fig. 3d and Supplementary Fig. S8). A stable ternary BCN alloy should have a BC$_x$N composition, that is, equal number of B and N atoms to fulfil charge neutrality conditions. Although different carbon concentrations BC$_x$N ($0.6 < x < 7$) have been reported, the most stable composition is believed theoretically to be BC$_2$N. There exist several types of isomers for BC$_2$N sheets derived from the substitution of a B–N pair for C$_2$, whereby the energetics is determined by competition between structural stress and chemical bond strength. Owing to the distinguishable elemental contrast in STM imaging of h-BC$_2$N, several isomers can be identified. Two isomers were found to be dominant structures in Fig. 3h, which match the two
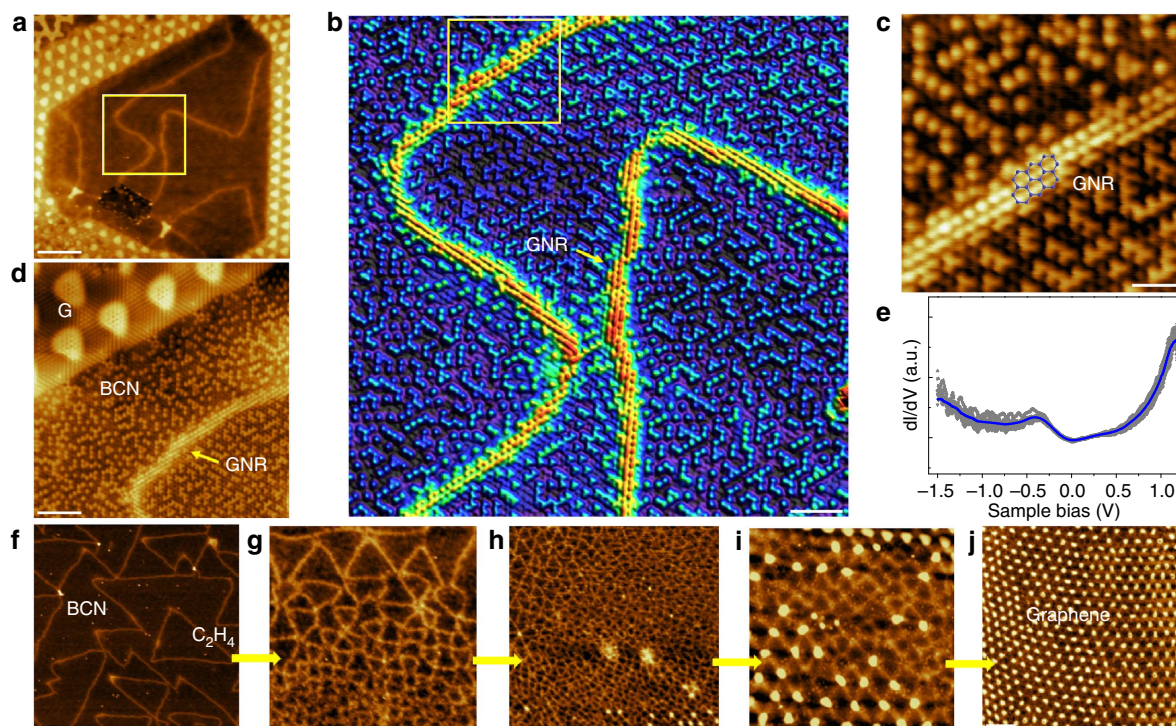
Figure 2 | Atomic structure and electronic property of GNRs. (**a**) STM image of etched G-Ru into GNRs embedded in BCN domains. (**b**) Magnified view of the square-enclosed region in (**a**) (GNR shows an apparent height of 0.5 Å). (**c**) Magnified view of the square-enclosed region in **b** to show the atomic structure of GNR. (**d**) The grain boundaries of G moiré and etched G (B–C–N domain coherently intergrown with GNRs). (**e**) A gap-like feature is present in the STS curve of GNRs. (**f–j**) STM images of the evolution of GNRs and segregated G moiré phases upon the stepwise dosing of ethene at 900 K. Scale bars in **a–d**: 6, 1.5, 0.5 and 3 nm, respectively; in **f–h**, **j**: 10 nm; in **i**: 4 nm.

most stable configurations among various h-BC$_2$N polymorphic structures predicted by Liu *et al.*[5] and Lu *et al.*[22] In type I isomer (inset in the right corner of Fig. 3h), the unit cell contains eight atoms and each C atom has a C, B and N nearest neighbour, whereas each B (N) has two C and one N (B) as nearest neighbours. This model has inversion symmetry allowing all the bond lengths to be relaxed and thus the structural stress is minimized. In contrast, in type II isomer (inset in the bottom of Fig. 3h), each C atom is joined to two other C atoms and either one B or N, whereas each B (N) atom has two N (B) neighbour coordination leading to chains of C and BN. This atomic arrangement in type II possesses optimized chemical bond energy, which is predicted to be the most energetically favourable isomer, consistent with the observation chains of carbon in Fig. 3b,c. According to previous calculations, the total energy difference between these two isomers is only ∼0.18 eV per unit cell[5], thus coexistence is possible at the growth temperature of 900 K.

Description of brick-and-mortar structures. Interestingly, we found that the complex phase-separation behaviours observed can be explained using classic BEG model[16] in a 2D honeycomb lattice consisting of C, B and N atoms on Ru surface. Each site of this lattice can be occupied by one of these atoms whose states are represented by a variable S_i ($S_i = 0, +1$ and -1 for C, B and N atoms, respectively). We do not consider the presence of vacancies because those are rarely seen in the experiments. There are six different important short range attractive potentials, $V_{\alpha\beta} > 0$, ($\alpha, \beta =$ B, C, N) that describe the energetics of the problems, which is consistent with the proposed models used in Chacham's work[7,9]. Taking into account the chemical potentials μ_α for each atomic species, it can be shown that within this model

the energy of the alloy can be written as follows:

$$E = \sum_{<i,j>} [KS_i^2 S_j^2 + JS_iS_j + L(S_i^2 S_j + S_j^2 S_i)] - H\sum_i S_i + \Delta \sum_i S_i^2 \quad (2)$$

where $<i,j>$ indicates the sum over nearest neighbour atoms in the honeycomb lattice and $K = ((V_{cc}/4) - (V_{BN}/2) + V_{CN} + V_{BC} - (V_{BB}/4) - (V_{NN}/4))$, $J = (V_{BN}/4) - (V_{NN}/4) - (V_{BB}/4)$, $L = (V_{CN}/2) - (V_{BC}/2) - (V_{NN}/4) - (V_{BB}/4)$, $H = (\mu_N - \mu_B)/2$ and $\Delta = \mu_C - (\mu_N + \mu_B)/2$. Equation (2) describes the BEG model used for the study of the λ transition in He^3–He^4 mixtures. In the current situation, where $V_{BN} \gg V_{NN}, V_{BB}$, we have $J > 0$ which is also known as the Spin-1 antiferromagnetic Ising model[23]. The honeycomb lattice can be divided into two interpenetrating triangular lattices labelled with $a = 1,2$. For each sublattice, the density of atomic species is given by: $\rho_{C,a} = \sum_{i\in a} (1 - <S_i^2>)/N$, $\rho_{B,a} = \sum_{i\in a} <S_i(S_i - 1)>/2N$ and $\rho_{N,a} = \sum_{i\in a} <S_i(S_i + 1)>/2N$ (equation (2)), where N is the total number of sites in each sublattice and the angular brackets represent ensemble averages (notice that owing to the absence of vacancies: $\rho_{C,a} + \rho_{B,a} + \rho_{N,a} = 1$). The order parameters for this problem are: $q = \sum_{a=1,2}(\rho_{B,a} + \rho_{N,a})$ that describes total BN density; $m = \sum_{a=1,2}(\rho_{N,a} - \rho_{B,a})$ that describes the total BN composition; $q_s = (\rho_{N,1} + \rho_{B,1} - \rho_{N,2} - \rho_{B,2})/2$ that describes the difference in BN density in the two sublattices; $m_s = (\rho_{N,1} + \rho_{B,2} - \rho_{N,2} + \rho_{B,2})/2$ that describes the difference in BN composition in the two sublattices. The set of numbers (q, q_S, m, m_S) describes all the possible thermodynamic phases. Crystalline BN phase is described by $(1, 0, 0, \mp 1)$ (notice that this is a doubly degenerated phase as we have two different choices for the B and N atoms in sublattices 1 and 2), whereas disordered BN is given by $(1, 0, 0, 0)$. Graphene is given by $(0, 0, 0, 0)$, that is, it is the vacuum phase. Hence, we can have a transition between graphene
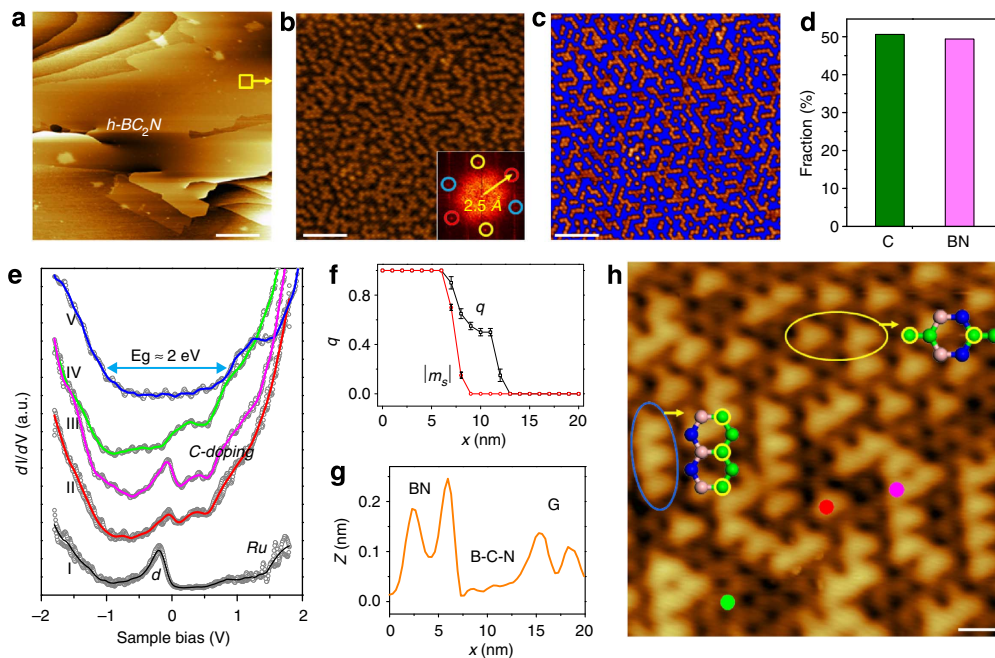
　　　　　　　　　　　　　　　　　　　　　　　　　　　　ARTICLE

Figure 3 | Atomic structure and electronic properties of h-BC2N film. (**a**) Extended h-BC_2N film grown by the sequential dosing of ethene; (5L) and borazine (15L) at 750–800 K. Scale bar, 200 nm. (**b**) A magnified view of BC_2N film in **a** (square-enclosed region), where the bright spots indicate carbon atoms in the BN matrix (dark background). (Inset: FFT shows the anisotropic arrangement of bright spots in $<11\bar{2}0>$ directions.) (**c**) STM image of **b** was processed using the flooding analysis function in Wsxm software for stoichiometrical analysis. (**d**) Stoichiometrical h-BC_2N is revealed by the analysis of the ratio between the integrated areas of bright dots (carbon) and dark regions (BN) (1:1). (**e**) The dI/dV spectra collected at bare Ru (I), (II) bright spot (red spot in **h**); (III), bright clusters (pink spot in **h**); (IV), dark region (marked in green spot in **h**); and (V); decoupled BCN in Supplementary Fig. S10. (**f**–**g**) The order parameters (q, m_s) determined in G, BN and mixed BCN zones (error bar represents the standard deviation of order-parameter measurements in three different regions; see Supplementary Fig. S9 for details) . (**h**) Atomic imaging of h-BC_2N and reveal two most stable isomer structure with its corresponding structure illustrated in the inset. Green = C atoms, blue = N atoms and grey = B atoms. Scale bar in **b**,**c**: 3 nm; in **h**: 2.5 Å. One bright spot in **h** corresponds to one C–C pair on the imaged triangular lattice, whereby the zigzag bright structures are assigned to the zigzag carbon chains in isomer II, and the other spaced-apart bright spots are assigned to isomer I. Bright and dark spots in **c** form a triangular lattice which indicates the lattice symmetry in h-BC_2N is broken owing to the interaction with Ru substrate.

to either ordered or disordered BN. The complexity of the phase diagram comes from the competition between the K and J terms in equation (2). Although the K term favours a graphene phase, the J term favours a crystalline BN phase. In the case where the concentration of B and N is the same we have, by symmetry, $H = m = q_s = 0$. In this case, as K and J are fixed, the phase diagram is controlled by Δ. When $\Delta \mapsto -\infty$ the system is pure BN (no C), whereas in the opposite limit of $\Delta \mapsto +\infty$ the system is pure C (no BN). At a critical value of $\Delta = \Delta_C$ there is a first-order phase transition between these two phases with a coexistence phase in between. This model is highly consistent with the experimental observations. As shown in Fig. 3f, the order parameters (q, m_S) determined in pure BN and graphene zones are (1, ±1) and (0, 0), respectively, whereas it changes to (0.5, 0) in the central region of the B–C–N zones sandwiched between G and BN (Fig. 3g), indicating the formation of a stoichiometric h-BC_2N alloy phase (Supplementary Fig. S9). In the coexistence phase, there are interfaces between locally ordered regions separated by domain walls oriented 60° from each other, leading to the formation of brick-and-mortar structure that we observe. The kinetics of growth is driven by the motion of such domain walls that interpolate one phase to the other[24]. The observed GNRs are the solitons of such interfaces[25].

Electronic properties of h-BC2N by STS. The electronic structures of h-BC_2N before and after decoupling from the Ru substrate are investigated using STS (Fig. 3e). The STS spectrum of clean Ru surface shows a characteristic d state at ~ 0.4 eV (ref. 26). Upon the growth of a layer of h-BC_2N, the d state from Ru is quenched and in the STS spectrum recorded at the bright spots, a new carbon-induced midgap state appears at -0.1 eV (Fig. 3e); this feature is conspicuously absent in the spectra collected at the dark area (pure BN region). Both spectra display gap-like features but with non-zero tunnelling conductance within the gap owing to the interfacial hybridization between BCN with Ru atoms. To eliminate the substrate effect, the h-BC_2N domain is decoupled from the metal surface by oxygen intercalation, this is a common strategy used for the delamination of graphene on metal substrate[27,28] (Supplementary Fig. S10). Upon the intercalation, the observed corrugation of h-BC_2N vanishes and an energy gap of 2 eV is now observed in the averaged STS data. It is worth noting that the theoretically predicted band gap is 1.6 eV for the most stable h-BC_2N configuration[5,10,14].

Although the BCN system is predicted to be driven towards segregation of pure C and BN patches in the thermodynamic limit[29], a complete solid miscibility between C and BN to form percolated h-BC_2N domain can be attained under thermodynamically non-equilibrium conditions, that is, the growth temperature should be lowered to impede the segregation of solute atoms but high enough to overcome the energy barrier of mixing, in combination with the rapid quenching from this growth temperature to fossilize the randomly distributed solute atoms. To suppress the phase segregation of carbon solute, a lower growth temperature coupled with a two-stage enrichment of the elements is needed. The energy barrier of mixing B–C–N

atoms to form h-BC$_2$N can be reduced by the pre-adsorption of C$_2$H$_4$ gas on Ru(0001). Micron-sized h-BC$_2$N domains are successfully grown by pre-adsorbing one monolayer C$_2$H$_4$ on Ru(0001), followed by annealing in borazine atmosphere at 750–800 K (Fig. 3a).

Spatially patterned lateral graphene and h-BC$_x$N heterostructures. According to the metal-catalysed substitution mechanism observed here, BN or G monolayer on metal is a versatile template for the fabrication of hybrids because diffusion of B/N or carbon precursors into the host matrix via grain boundaries or exposed edges results in substitutional exchange. Similar to the substitutional exchange of existing graphene islands into BC$_x$N, our STM results show that pre-existing BN islands on Ru can also be transformed into mixed BCN phases when the sample is exposed to C$_2$H$_4$ gas at 900 K (Supplementary Fig. S11). To test the generic validity of the proposed lattice substitutional model we have observed for G/BN on Ru, we have performed similar patterned re-growth experiments on both Ru and Pt metal substrates and transferred the films onto SiO$_2$ for characterization. As shown in Fig. 4 and Supplementary Fig. S12, parallel h-BN strips pre-grown on Pt or Ru substrate were achieved by spatial patterning. The h-BN strips, alternating with bare Pt and Ru regions, were then exposed to ethylene. After the reaction, a continuous film consisting of laterally joined h-BC$_x$N and G parallel strips was grown (schematic in Fig. 4a). The film was electrochemically exfoliated from the metal substrate and transferred onto a SiO$_2$/Si substrate for optical characterization. Figure 4b,c shows the optical contrast arising from alternating graphene (grown on bare Pt) and h-BC$_x$N gratings, the spatial distribution of the h-BC$_x$N and G phases can be confirmed by Raman and photoluminescence (PL) mapping (Fig. 4d,e). In the BC$_x$N region, we observe strong PL signal located at around 590 nm (2.1 eV) when excited by a continuous wave laser (wavelength: 532 nm; Fig. 4f), whereas the graphene region is non-emissive, thus giving rise to bright and dark contrast in PL mapping. Similar results were obtained for the hybrid film grown on Ru, which suggests that the substitutional alloy of BN and G into BCN phase may have genetic validity for some transition metal substrates. The energy of the PL peak is assigned to BC$_2$N (ref. 14) and corresponds well to the bandgap of ~ 2 eV measured by the STS on the h-BC$_2$N area. It is worth noting that on a pure h-BN film, no PL signal (Supplementary Fig. S13) was obtained using visible light excitation, therefore the PL observed here originates from hybridized states formed between BN and C in BC$_x$N. The PL emission becomes saturated with increasing laser power (Fig. 4g), which suggests that the process is carrier-limited and related to some defect or impurity states[30]. The PL transient dynamics in h-BC$_x$N was also studied by time-resolved PL. Figure 4h shows the decay trace of the PL obtained at temperature of 80 K. Inset is the corresponding streak camera image of the transient PL decay dynamics. The PL decay profile can be fitted biexponentially, from which we obtained two distinct lifetimes of 450 ± 40 ps and 50 ± 10 ps (Supplementary Fig. S14) – originating from two carrier relaxation pathways.

Discussion

In summary, dynamic biphasic mixing and demixing in 2D ternary h-BC$_x$N system, catalysed by the metal substrate, has been studied at the atomic level using STM. The presence of a metallic catalyst lowers the energy for intermixing in 2D ternary system. Metal substrate-catalysed substitutional exchange of h-BN by carbon atoms, or graphene by B–N atoms, presents a route for doping and alloying under non-equilibrium conditions. The complex phase-separation behaviours observed can be rationalized using BEG model in a 2D honeycomb lattice. It can be expected that the mechanical strength and sheet conductance of the hybrid ternary film can be tailored by engineering the mortar, that is, the GNR network, surrounding the BN bricks. The results here demonstrate the amazing structural and compositional
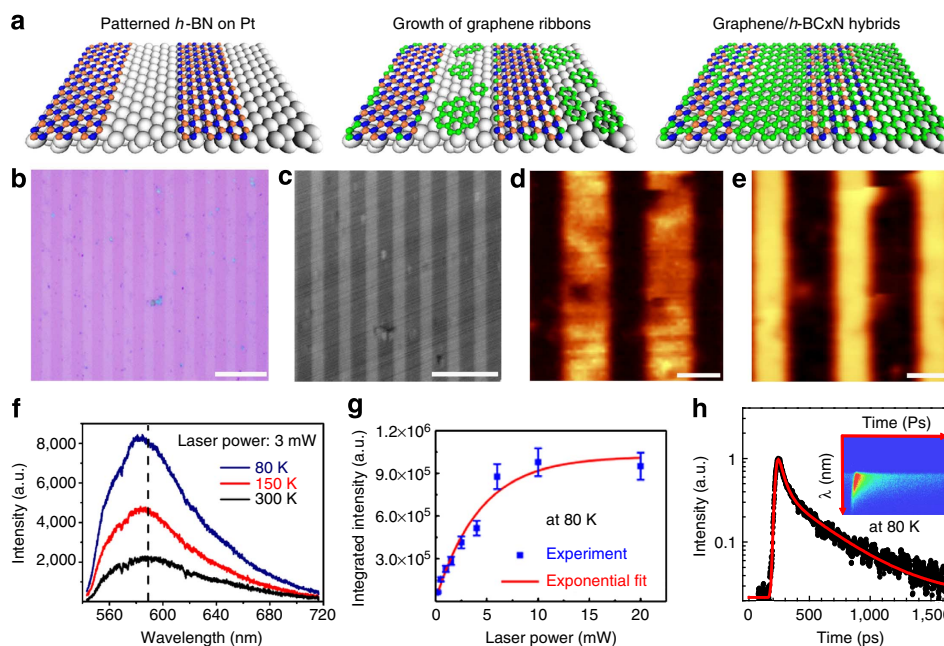

Figure 4 | Spatially patterned lateral graphene/h-BC$_x$N heterostructure. (**a**) Schematics of spatially patterned growth of lateral graphene/h-BC$_x$N heterostructure. (**b–c**) Optical and s.e.m. images of the lateral gratings with 2 μm period. Scale bars, 10 μm. (**d–e**) Raman (G band) and PL (590 nm band) mappings. Scale bars, 2 μm. (**f**) PL spectra recorded on the h-BC$_x$N film at different temperatures. (**g**) Excitation laser power dependent of the PL intensity. (**h**) Time-resolved PL decay dynamics of the h-BC$_x$N film – taken over the peak region. Inset shows the transient PL decay image taken with a long-pass filter (532 nm) to eliminate the excitation laser line.

versatility of graphene (or h-BN) monolayer on metal where the fabrication of h-BC$_2$N nanostructures integrated with GNRs can be achieved by direct substitution reactions.

Methods

Sample preparation and STM characterization. The experiments were performed in an ultrahigh vacuum chamber equipped with an STM and an adjoined sample preparation chamber, with a base pressure of 1.5×10^{-10} mbar. The Ru(0001) surface was carefully cleaned using standard recipe[24]. The clean Ru(0001) was exposed to a gas flux of C$_2$H$_4$ gas (National Oxygen Pte Ltd., purity 99.99%) at a partial pressure of 1×10^{-7} mbar for 10 min with the substrate heated up to ~ 900–1,000 K to grow submonolayer graphene (~ 0.7–0.8 Ml). To synthesize the brick-and-mortar pattern consisting of mixed BC$_2$N phase and GNRs, as-prepared graphene/Ru(0001) was annealed in vaporized borazine with a partial pressure of $\sim 2 \times 10^{-8}$ mbar for 5 min. After growth, the sample was characterized by a SPECS STM 150 Aarhus unit with the Nanonis (SPECS) SPM control system at 298 K.

Patterned regrowth of graphene/h-BC$_x$N heterostructures. The growth of spatially patterned lateral graphene/h-BC$_x$N heterostructure was carried out in the ultrahigh vacuum condition on platinum (Pt) foil and Ru single crystal using the same precursors as above. The h-BN film grown on Pt film or Ru was patterned into 2 μm strips with alternate 2 μm spacing by nano-imprinting. The patterned h-BN film on Pt foil or Ru crystal was then placed in 1-methyl-2-pyrrolidone to clean away residual resist. Next, graphene was deposited by CVD on the bare metal surface between the h-BN strips. Finally, the lateral graphene/h-BC$_x$N heterostructure films were electrochemically delaminated from the Pt foils or Ru crystal for further characterizations (refer to details in supporting information).

PL measurement. Spatially resolved PL measurements of the as-prepared samples were performed using a confocal microscope with a long working distance 50× objective (Nikon Objective, NA = 0.55) and a continuous wave laser (532 nm wavelength) as the excitation source. The PL emission was spectrally resolved with a monochromator (PI Acton, Spectra Pro 2500i) and collected with a thermoelectrically cooled charged coupled device camera (PI, PIXIS-400B). Temperature-dependent PL (77–300 K) was performed using a liquid-nitrogen-cooled cryostat (Janis, ST-500 Microscope Cryostat). For time-resolved PL measurements, frequency doubled pulses (400 nm) from a Coherent Mira Titanium:Sapphire oscillator (120 fs, 76 MHz at 800 nm) was used as the excitation source. The time-resolved PL spectra were obtained using a streak camera system (Optronis GmbH) configured with a fast synchroscan sweep unit (FSSU1-ST) which has an ultimate temporal resolution of ~ 2 ps including jitter (or ~ 6 ps after coupling with a monochromator) at the fastest scan speed of 15 ps mm^{-1}. Typical operating scan speeds in this work was at 100 ps mm^{-1}.

References

1. Stephan, O. *et al.* Doping graphitic and carbon nanotube structures with boron and nitrogen. *Science* **266**, 1683–1685 (1994).
2. Ayala, P., Arenal, R., Loiseau, A., Rubio, A. & Pichler, T. The physical and chemical properties of heteronanotubes. *Rev. Mod. Phys.* **82**, 1843–1885 (2010).
3. Ci, L. *et al.* Atomic layers of hybridized boron nitride and graphene domains. *Nat. Mater.* **9**, 430–435 (2010).
4. Arenal, R., Blase, X. & Loiseau, A. Boron-nitride and boron-carbonitride nanotubes: synthesis, characterization and theory. *Adv. Phys.* **59**, 101–179 (2010).
5. Liu, A. Y., Wentzcovitch, R. M. & Cohen, M. L. Atomic arrangement and electronic-structure of BC$_2$N. *Phys. Rev. B* **39**, 1760–1765 (1989).
6. Bernardi, M., Palummo, M. & Grossman, J. C. Optoelectronic properties in monolayers of hybridized graphene and hexagonal boron nitride. *Phys. Rev. Lett.* **108**, 226805-1–226805-5 (2012).
7. Mazzoni, M. S. C., Nunes, R. W., Azevedo, S. & Chacham, H. Electronic structure and energetics of B$_x$C$_y$N$_z$ layered structures. *Phys. Rev. B* **73**, 073108-1–073108-4 (2006).
8. Liu, Y. Y., Bhowmick, S. & Yakobson, B. I. BN white graphene with 'colorful' edges: the energies and morphology. *Nano Lett.* **11**, 3113–3116 (2011).
9. Martins, J. D. & Chacham, H. Disorder and segregation in B-C-N graphene-type layers and nanotubes: tuning the band gap. *Acs Nano* **5**, 385–393 (2011).
10. Nozaki, H. & Itoh, S. Lattice dynamics of BC$_2$N. *Phys. Rev. B* **53**, 14161–14170 (1996).
11. Sutter, P., Cortes, R., Lahiri, J. & Sutter, E. Interface formation in monolayer graphene-boron nitride heterostructures. *Nano Lett.* **12**, 4869–4874 (2012).
12. Levendorf, M. P. *et al.* Graphene and boron nitride lateral heterostructures for atomically thin circuitry. *Nature* **488**, 627–632 (2012).
13. Liu, Z. *et al.* In-plane heterostructures of graphene and hexagonal boron nitride with controlled domain sizes. *Nat. Nanotech.* **8**, 119–124 (2013).
14. Watanabe, M. O., Itoh, S., Sasaki, T. & Mizushima, K. Visible-light-emitting layered BC2N semiconductor. *Phys. Rev. Lett.* **77**, 187–189 (1996).
15. Chen, Y., Barnard, J. C., Palmer, R. E., Watanabe, M. O. & Sasaki, T. Indirect band gap of light-emitting BC2N. *Phys. Rev. Lett.* **83**, 2406–2408 (1999).
16. Blume, M., Emergy, V. J. & Griffith, Rb Ising model for lambda transition and phase separation in He-3-He-4 mixtures. *Phys. Rev. a-Gen. Phys.* **4**, 1071–1077 (1971).
17. Sadigh, B. *et al.* Short-range order and phase stability of surface alloys: PdAu on Ru(0001). *Phys. Rev. Lett.* **83**, 1379–1382 (1999).
18. Tersoff, J. Surface-confined alloy formation in immiscible systems. *Phys. Rev. Lett.* **74**, 434–437 (1995).
19. Shelton, J. C., Patil, H. R. & Blakely, J. M. Equilibrium segregation of carbon to a nickel (111) surface – surface phase-transition. *Surf. Sci.* **43**, 493–520 (1974).
20. Thompson, K., Flaitz, P. L., Ronsheim, P., Larson, D. J. & Kelly, T. F. Imaging of arsenic Cottrell atmospheres around silicon defects by three-dimensional atom probe tomography. *Science* **317**, 1370–1374 (2007).
21. Goriachko, A. *et al.* Self-assembly of a hexagonal boron nitride nanomesh on Ru(0001). *Langmuir* **23**, 2928–2931 (2007).
22. Lu, P., Zhang, Z. H. & Guo, W. L. Electronic structures of BC2N nanoribbons. *J. Phys. Chem. C* **115**, 3572–3577 (2011).
23. Saito, Y Spin-1 anti-ferromagnetic Ising-model. 1. Bulk phase-diagram for a binary alloy. *J. Chem. Phys.* **74**, 713–720 (1981).
24. Saito, Y. & Mullerkrumbhaar, H. Anti-ferromagnetic spin-1 Ising-model. 2. Interface structure and kinetic phase-transition. *J. Chem. Phys.* **74**, 721–727 (1981).
25. Langer, J. S. Theory of spinodal decomposition in alloys. *Ann. Phys-New York* **65**, 53–86 (1971).
26. Gyamfi, M., Eelbo, T., Wasniowska, M. & Wiesendanger, R. Inhomogeneous electronic properties of monolayer graphene on Ru(0001). *Phys. Rev. B* **83**, 153418-1–153418-4 (2011).
27. Zhang, H., Fu, Q., Cui, Y., Tan, D. L. & Bao, X. H. Growth mechanism of graphene on Ru(0001) and O-2 adsorption on the graphene/Ru(0001) surface. *J. Phys. Chem. C* **113**, 8296–8301 (2009).
28. Lu, J., Neto, A. H. C. & Loh, K. P. Transforming moire blisters into geometric graphene nano-bubbles. *Nat. Commun* **3**, 823 (2012).
29. Blase, X., Charlier, J. C., De Vita, A. & Car, R. Structural and electronic properties of composite BxCyNz nanotubes and heterojunctions. *Appl. Phys. A Mater. Sci. Process.* **68**, 293–300 (1999).
30. Park, J. H., Lee, T. K., Noh, Y. K., Kim, M. D. & Oh, E. Temperature and excitation power dependence of photoluminescence from high quality GaSb grown on AlSb and GaSb buffer layers. *J. Appl. Phys.* **105**, 043516-1–043516-4 (2009).

Acknowledgements

Author contributions

J.L., K.Z. and K.P.L. conceived the original idea. J.L. carried out the STM experiments. K.Z. performed the growth of spatially G/h-BC$_x$N heterostructures. K.Z., X.F.L. and H.Z. measured PL. A.H.C.N. provided the theoretical framework. J.L., K.Z., X.F.L., T.C.S. and K.P.L. analysed the data and discussed the results. J.L., K.Z, A.H.C.N and K.P.L wrote the manuscript. All authors discussed and commented on the manuscript.

Additional information